Large-excitability asymptotics for scroll waves in three-dimensional excitable media

Daniel Margerit* and Dwight Barkley†
Mathematics Institute, University of Warwick, Coventry CV4 7AL, United Kingdom
(Received 23 March 2001; revised manuscript received 29 April 2002; published 23 September 2002)

Three-dimensional scroll waves are considered in a reaction-diffusion model of excitable media in the large excitability limit. Coordinates based on the scroll filament are defined and shown to provide a natural extension of the coordinates used for two-dimensional spiral waves. The leading-order free-boundary equations for interface motion in three dimensions are explicitly derived in these coordinates. Three specific examples are considered: straight twisted scroll waves, axisymmetric scroll waves, and helical scroll waves. The equations for the fields at leading and first order in the core region are given.

DOI: 10.1103/PhysRevE.66.036214 PACS number(s): 82.40.Ck, 47.54.+r, 87.10.+e

I. INTRODUCTION

Wave propagation in excitable media occur in a wide variety of chemical and biological contexts [1–4], the most important example being the electrical wave propagation in heart tissue [5–8]. In three-dimensional media, one typically finds sustained waves in the form of scrolls that rotate about one-dimensional filaments (Fig. 1). These filaments can themselves move through the medium, generally on a time scale much slower than the time scale of wave rotation about the filament, e.g., Refs. [9–13]. Almost all current theoretical understanding of scroll wave dynamics in excitable media is based on laws that have been derived for the motion of filaments [9,14–18]. However, as we explain below, this theory is incomplete and does not include a description of scroll waves themselves. In this paper we derive general asymptotic equations for three-dimensional (3D) scroll waves directly from reaction-diffusion partial-differential equations and consider these equations in specific cases for which the equations simplify.

We consider a standard two-component reaction-diffusion model of excitable media:

$$\varepsilon^2 \partial u/\partial t = \varepsilon^2 \nabla^2 u + f(u,v), \tag{1a}$$

$$\partial v/\partial t = \varepsilon g(u,v). \tag{1b}$$

The equations are here written in the space and time scales proposed by Fife [19]. The small parameter ε is the characteristic time scale separation between the fast u species and the slow v species. This scale separation is exploited in our analysis. For concreteness we consider specific reaction terms [20–22]:

$$f(u,v) = u(1-u)\left(u - \frac{v+b}{a}\right), \tag{2a}$$

$$g(u,v) = u - v, \tag{2b}$$

where a and b are parameters. Our analysis applies equally to all similar two-component reaction-diffusion equations.

Previous analytical work on the motion of scroll filaments has been of two types. The first one is strictly phenomenological [23–28], using geometrical considerations only and not relying directly on the underlying reaction-diffusion equations. The second approach is based on reaction-diffusion equations and uses singular perturbation theory [14,16,18] in the *small filament curvature limit*. (The filament torsion is also assumed to be small [except in Ref. [29]], but for simplicity we shall refer only to filament curvature.) The parameter ε controlling excitability is fixed and then the small (order-δ) curvature limit is considered. Significantly, it must be assumed that the solution to the reaction-diffusion equations for a straight filament (equivalent to the two-dimensional spiral solution) is known for any required ε. This is the leading-order ($\delta=0$) solution. Equations for filament motion on a small (order-δ) velocity scale are then obtained by invoking a compatibility condition for the equations at first order in δ. In this work it has not been

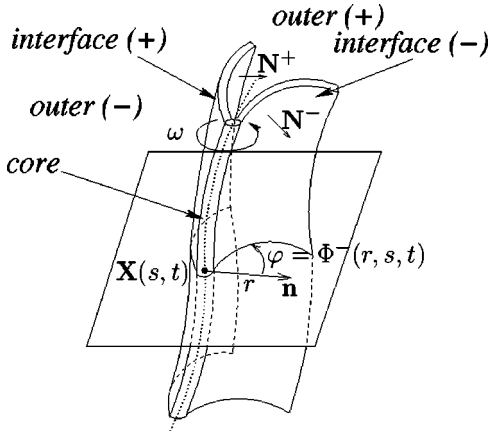

FIG. 1. Sketch of a rotating scroll wave showing the different asymptotic regions and the coordinates used. Shown are the outer regions [excited (+) and quiescent (−)], the interface regions [wave front (+) and wave back (−)], and the core region. The filament $\mathbf{X}(s,t)$ is parametrized by s and time t. Local coordinates to the filament are (r,φ,s), with (r,φ) in the plane normal to $\mathbf{X}(s,t)$ and φ is measured from the normal vector $\mathbf{n}$. The wave rotates about the filament. The interface normals $\mathbf{N}^{\pm}$ are also displayed.

*Present address: Institut de Mécanique des Fluides de Toulouse, 31400 Toulouse Cedex, France. Email address: margerit@imft.fr
†Email address: barkley@maths.warwick.ac.uk

 ©2002 The American Physical Society

possible to find the left null eigenvectors of the relevant linear operator and to show that the orthogonal product of these vectors on the nonhomogeneous terms yields nonvanishing equations of motion. Therefore the order-δ velocity of the filament has not been substantiated, and more importantly, the coefficients of the equations of motion are not given as functions of the parameters of the original reaction-diffusion system, e.g., Eqs. (1). The analysis is nevertheless very important because it gives the form of the equations of motion at lowest order.

Since the early pioneering work on filament motion in excitable media and on 2D spiral waves [30–32], the stationary (rigidly rotating) 2D spiral has been fully understood using singular perturbation methods, both at leading order in ε [33–39] and more recently at first order in ε [40,41]. Scroll waves with straight filaments can be understood in the same way [37,40,41]. Progress has also been made in understanding spiral drift, in the small-ε limit, in bounded domains [42], and with applied fields [43]. Using a slightly different approach [44,45], the $\varepsilon \to 0$ limit is considered while the medium is kept in the weakly excitable regime [46].

The purpose of this paper is to build on the understanding gained from the two-dimensional case and to present a general geometrical description for three-dimensional scroll waves in the small-ε limit. Specifically we will define a useful system of three-dimensional coordinates and derive free-boundary equations for wave motion in these coordinates. If curvature and twist (as defined later in Sec. IV C) are taken to zero, the known equations for stationary spirals are automatically recovered. In this approach, it is not necessary at the outset to assume small filament curvature, and the equations are equally valid for large and small curvatures.

II. ASYMPTOTIC EQUATIONS

The first step in the analysis is to specify the geometry of the problem and to identify the different asymptotic regions to be considered. The coordinate system we use is based on the scroll filament (Fig. 1). Let the filament be a curve $\mathcal{C}$ given parametrically by coordinate s and time t: $\mathbf{X} = \mathbf{X}(s,t)$. Local to the filament we shall use the coordinate frame $(\mathbf{e}_r, \mathbf{e}_\varphi, \mathbf{t})$, where $(\mathbf{e}_r, \mathbf{e}_\varphi)$ are unit vectors associated with polar coordinates (r,φ) in the plane normal to the filament with φ measured from the normal $\mathbf{n}$ to $\mathcal{C}$, and $\mathbf{t}$ is the unit tangent vector. Then points $\mathbf{x}$ local to $\mathcal{C}$ are given in (r,φ,s) coordinates by

$$\mathbf{x}(r,\varphi,s,t) = \mathbf{X}(s,t) + r\mathbf{e}_r(\varphi,s,t).$$

We use polar coordinates rather than Cartesian coordinates (built on the normal and binormal frame) as used by Keener [14] because the 2D spiral equations written in polar coordinates are then easily recovered with our treatment. The medium divides into three regions (Fig. 1): outer, interface, and core. The outer region comprises most of the medium. It is itself divided into both an *excited* portion, for which $u \simeq 1$, and a *quiescent* portion, for which $u \simeq 0$. The interface region is a thin (quasi-two-dimensional) region separating the excited and quiescent portions of the outer region. In the interface region, u makes a rapid change between $u=0$ and $u=1$. On the outer scale, this interface region is a surface $\mathcal{S}$, the scroll surface. For concreteness, we define $\mathcal{S}$ to be the surface $u=1/2$. It consists of two parts: a *wave front* and a *wave back* described, respectively, by two functions $\Phi^{\pm}$; such that $\varphi = \Phi^{\pm}(r,s,t)$. Finally, when it exists, the core region is a small quasi-one-dimensional region containing the filament. Tyson and Strogatz [47] reviewed the geometrical description of the filament including twist. Here, the differential geometry of the scroll wave includes additionally the interfaces $\Phi^{\pm}$.

In the small-ε limit, both the filament position $\mathbf{X}$ and the interface depend on ε, and have expansions of the form

$$\mathbf{X}(s,t,\varepsilon) = \mathbf{X}^{(0)}(s,t) + \varepsilon \mathbf{X}^{(1)}(s,t) + \cdots,$$

$$\Phi(r,s,t,\varepsilon) = \Phi^{(0)}(r,s,t) + \varepsilon \Phi^{(1)}(r,s,t) + \cdots,$$

where Φ means either Φ^+ or Φ^-. We refer to these orders as *leading order*, *first order*, etc.

The next step in the analysis is to rewrite Eqs. (1) in each of the three regions—outer, interface, and core—using appropriate coordinates. From these equations one can obtain a hierarchy of asymptotic equations in each region.

A. Outer region

In the outer region, we write Eqs. (1) in (r,φ,s) coordinates:

$$\varepsilon^2 \partial u/\partial t = \varepsilon^2 \nabla^2 u + f(u,v) + \varepsilon^2 \mathbf{v_f} \cdot \boldsymbol{\nabla} u, \tag{3a}$$

$$\partial v/\partial t = \varepsilon g(u,v) + \mathbf{v_f} \cdot \boldsymbol{\nabla} v, \tag{3b}$$

where $\mathbf{v_f} = \dot{\mathbf{X}} + r\dot{\mathbf{e}}_r$ is the velocity of the moving frame due to filament motion.

The gradient operator in these coordinates is

$$\boldsymbol{\nabla} = \mathbf{e}_r \frac{\partial}{\partial r} + \mathbf{e}_\varphi \frac{1}{r} \frac{\partial}{\partial \varphi} + \mathbf{t}\mathcal{H}$$

and the Laplacian is

$$\nabla^2 = \frac{1}{rh} \frac{\partial}{\partial r}\left(rh \frac{\partial}{\partial r}\right) + \frac{1}{r^2 h} \frac{\partial}{\partial \varphi}\left(h \frac{\partial}{\partial \varphi}\right) + \mathcal{H}\mathcal{H},$$

where

$$\sigma \equiv |\partial \mathbf{X}/\partial s|,$$

$$h \equiv \sigma(1 - r\kappa \cos\varphi),$$

$$\mathcal{H} \equiv \frac{1}{h}\left(\frac{\partial}{\partial s} - \sigma\tau \frac{\partial}{\partial \varphi}\right).$$

Here, κ is the curvature and τ is the torsion of the filament. Details can be found in the Appendix.

We write the expansions for u and v in the outer region in the form

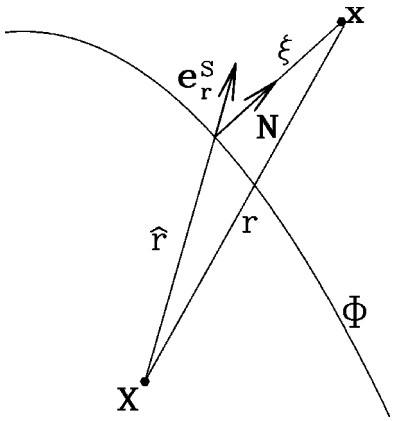

FIG. 2. Sketch showing definition of interface coordinates $\hat{r}$ and ξ ($\hat{s}$ is not illustrated).

$$u(r,\varphi,s,t,\varepsilon)=u^{(0)}(r,\varphi,s,t)+\varepsilon u^{(1)}(r,\varphi,s,t)+\cdots,$$

$$v(r,\varphi,s,t,\varepsilon)=v^{(0)}(r,\varphi,s,t)+\varepsilon v^{(1)}(r,\varphi,s,t)+\cdots.$$

Substitution of these expansions into Eqs. (3) gives a hierarchy of asymptotic equations for the orders $u^{(k)}$ and $v^{(k)}$, $k=0,1,\ldots,$ of the u and v fields in the outer region.

B. Interface region

For the interface region we shall use the local coordinates $(\hat{r},\hat{s},\xi)$ to describe the position of a point **x** near interface Φ. These coordinates are defined by projecting the point **x** to the interface along the interface normal **N** (see Fig. 2). Then ξ is the distance to the interface; $\hat{r}$ and $\hat{s}$ are the values of r and s of the projection onto the interface. Specifically, points **x** local to the interface are given in $(\hat{r},\hat{s},\xi)$ coordinates by

$$\mathbf{x}(\hat{r},\hat{s},\xi,t)=\mathbf{X}(\hat{s},t)+\hat{r}\mathbf{e}_r^{\mathbf{s}}(\hat{r},\hat{s},t)+\xi\mathbf{N}(\hat{r},\hat{s},t),$$

with $\mathbf{e}_r^{\mathbf{s}}(\hat{r},\hat{s},t)=\mathbf{e}_r[\Phi(\hat{r},\hat{s},t),\hat{s},t]$. For points **x** on the interface, $\xi=0$ and $(\hat{r},\hat{s})=(r,s)$.

In this interface regions, the stretched coordinate $\overline{\xi}=\xi/\varepsilon$ is then introduced, and in $(\hat{r},\hat{s},\overline{\xi})$ coordinates, Eqs. (1) become

$$\varepsilon^2\partial u/\partial t=\overline{\nabla}^2u+f(u,v)+\varepsilon\mathbf{v}\cdot\overline{\boldsymbol{\nabla}}u, \tag{4a}$$

$$\partial v/\partial t=\varepsilon g(u,v)+\varepsilon^{-1}\mathbf{v}\cdot\overline{\boldsymbol{\nabla}}v, \tag{4b}$$

where

$$\mathbf{v}=\mathbf{v}_\mathbf{f}^\mathbf{s}+\mathbf{v}_\mathbf{i}, \tag{5}$$

$$\mathbf{v}_\mathbf{f}^\mathbf{s}\equiv\dot{\mathbf{X}}+\hat{r}\dot{\mathbf{e}}_r^\mathbf{s} \tag{6}$$

$$\mathbf{v}_\mathbf{i}\equiv\hat{r}\dot{\Phi}\mathbf{e}_\varphi^\mathbf{s}+\varepsilon\overline{\xi}\dot{\mathbf{N}} \tag{7}$$

$$\overline{\nabla}=\varepsilon\nabla=\varepsilon\nabla_\pi+\mathbf{N}\frac{\partial}{\partial\overline{\xi}}, \tag{8}$$

$$\overline{\nabla^2}=\varepsilon^2\nabla^2=\varepsilon^2\nabla_\pi^2+\frac{\partial^2}{\partial\overline{\xi}^2}+\frac{1}{2m}\frac{\partial m}{\partial\overline{\xi}}\frac{\partial}{\partial\overline{\xi}}, \tag{9}$$

with $\mathbf{e}_\varphi^\mathbf{s}=\mathbf{e}_\varphi[\Phi(\hat{r},\hat{s},t),\hat{s},t]$ and $\dot{\mathbf{e}}_r^\mathbf{s}=\dot{\mathbf{e}}_r[\Phi(\hat{r},\hat{s},t),\hat{s},t]$. In Eq. (5), $\mathbf{v_i}$ is the contribution to the velocity of the moving frame coming from interface motion. The operators $\boldsymbol{\nabla}_\pi$ and ∇_π^2 are the gradient and Laplacian orthogonal to the **N** direction and m is the determinant of the metric tensor associated to the $(\hat{r},\hat{s},\overline{\xi})$ coordinates. The exact form of $\boldsymbol{\nabla}_\pi$ and ∇_π^2 are not required for the asymptotic orders considered in this paper. However, the lowest order representation of the last term in Eq. (9) is needed:

$$\frac{1}{2m}\frac{\partial m}{\partial\overline{\xi}}\frac{\partial}{\partial\overline{\xi}}=-\varepsilon 2H\frac{\partial}{\partial\overline{\xi}}+O(\epsilon^2), \tag{10}$$

where H is the mean curvature of the interface. Details of the interface coordinate system are given in the Appendix.

We write the expansions for u and v in the interface region as

$$u(\hat{r},\hat{s},\overline{\xi},t,\varepsilon)=u^{i(0)}(\hat{r},\hat{s},\overline{\xi},t)+\varepsilon u^{i(1)}(\hat{r},\hat{s},\overline{\xi},t)+\cdots,$$

$$v(\hat{r},\hat{s},\overline{\xi},t,\varepsilon)=v^{i(0)}(\hat{r},\hat{s},\overline{\xi},t)+\varepsilon v^{i(1)}(\hat{r},\hat{s},\overline{\xi},t)+\cdots,$$

where i denotes interface. Substitution of these expansions into Eqs. (4) gives a cascade of asymptotic equations for the orders $u^{i(k)}$ and $v^{i(k)}$, $k=0,1,\ldots,$ of the u and v fields in the interface region.

There are significant advantages to using the stretched normal coordinate to the interface $\overline{\xi}$ rather than the stretched relative angle to the interface $\overline{\varphi'}=(\varphi-\Phi)/\varepsilon$ used by Fife [30]. These advantages outweigh the fact that the change of coordinates in the Fife approach, between $(r,\overline{\varphi'},s)$ and the outer coordinates (r,φ,s), is simple. The problem with the Fife coordinates is that when the interface is expanded in ε, $\Phi(r,s,t,\varepsilon)=\Phi^{(0)}(r,s,t)+\varepsilon\Phi^{(1)}(r,s,t)+\cdots,$ (something not done by Fife), the solution of the kth-order equation for u across the interface is complicated in $(r,\overline{\varphi'},s)$ coordinates and both $\Phi^{(0)}$ and $\Phi^{(1)}$ enter in the first-order equation of $u^{i(1)}$, from which the equation for $\Phi^{(0)}$ must be extracted.

C. Core region

In the core region, the stretched radial coordinate $\overline{r}=r/\varepsilon$ is introduced. In $(\overline{r},\varphi,s)$ coordinates, Eqs. (1) become

$$\varepsilon^2\partial u/\partial t=\overline{\nabla}^2u+f(u,v)+\varepsilon\mathbf{v_f}\cdot\overline{\boldsymbol{\nabla}}u, \tag{11a}$$

$$\partial v/\partial t=\varepsilon g(u,v)+\varepsilon^{-1}\mathbf{v_f}\cdot\overline{\boldsymbol{\nabla}}v, \tag{11b}$$

where $\mathbf{v_f}=\dot{\mathbf{X}}+\varepsilon\overline{r}\dot{\mathbf{e}}_r$ and

$$\bar{\nabla} = \varepsilon \nabla = \mathbf{e}_r \frac{\partial}{\partial \bar{r}} + \mathbf{e}_\varphi \frac{\partial}{\bar{r} \partial \varphi} + \mathbf{t} \varepsilon \mathcal{H}$$

$$\bar{\nabla}^2 = \varepsilon^2 \nabla^2 = \frac{1}{\bar{r} h} \frac{\partial}{\partial \bar{r}} \left(\bar{r} h \frac{\partial}{\partial \bar{r}} \right) + \frac{1}{\bar{r}^2 h} \frac{\partial}{\partial \varphi} \left(h \frac{\partial}{\partial \varphi} \right) + \varepsilon^2 \mathcal{H} \mathcal{H}.$$

In $(\bar{r}, \varphi, s)$ coordinates $h = \sigma(1 - \varepsilon \bar{r} \kappa \cos \varphi)$. We write the expansions of u and v in this core region as

$$u(\bar{r}, \varphi, s, t, \varepsilon) = u^{c(0)}(\bar{r}, \varphi, s, t) + \varepsilon u^{c(1)}(\bar{r}, \varphi, s, t) + \cdots,$$

$$v(\bar{r}, \varphi, s, t, \varepsilon) = v^{c(0)}(\bar{r}, \varphi, s, t) + \varepsilon v^{c(1)}(\bar{r}, \varphi, s, t) + \cdots,$$

where c denotes core. Substitution of these expansions into Eqs. (11) gives a hierarchy of asymptotic equations for the orders $u^{c(k)}$ and $v^{c(k)}$, $k = 0,1, \ldots,$ of the u and v fields in the core region.

III. FREE-BOUNDARY EQUATIONS

The next step in the analysis is to solve the hierarchy of asymptotic equations in each of the asymptotic regions, order by order, and to apply appropriate matching between these regions. Sections III B and III C follow closely previous work [30–39].

A. Leading-order core

We begin with the core region. At lowest order (order ε^{-1}), Eq. (11b) for the v field in the core gives

$$\dot{\mathbf{X}}^{(0)} \cdot \bar{\nabla}^{c(0)} v^{c(0)} = 0, \tag{12}$$

where $\dot{\mathbf{X}}^{(0)}$ is independent of $\bar{r}$ and φ and

$$\bar{\nabla}^{c(0)} \equiv \mathbf{e}_r \frac{\partial}{\partial \bar{r}} + \mathbf{e}_\varphi \frac{\partial}{\bar{r} \partial \varphi}. \tag{13}$$

The simplest way to satisfy Eq. (12) is to assume no leading-order filament motion and set $\dot{\mathbf{X}}^{(0)} = 0$. Thus the filament velocity goes to zero in the limit $\varepsilon \to 0$. If, on the other hand, solutions to the reaction-diffusion equations exist with leading-order filament motion, $\dot{\mathbf{X}}^{(0)} \neq 0$, then $\bar{\nabla}^{c(0)} v^{c(0)}$ is a constant. Matching the core solution to the outer region (discussed in the following section) would, in fact, require $v^{c(0)}$ to be constant (and equal to the stall concentration as defined later in Sec. III B). It is known that v is not constant in the core of stationary (rigidly rotating) spirals in two dimensions [36,39]. Thus, while we cannot definitely rule out scroll solutions with leading-order filament motion, any such solution will be very different from the known two-dimensional spiral solutions that have cores with nonuniform fields $v^{c(0)}$. Direct numerical evidence that $\dot{\mathbf{X}}^{(0)} = 0$ for scroll rings is given in Ref. [41].

B. Leading-order outer and interface regions

At lowest order (order ε^0), Eqs. (3) give

$$0 = f(u^{(0)}, v^{(0)}), \tag{14}$$

$$\partial v^{(0)} / \partial t = 0. \tag{15}$$

Then $u^{(0)}$ is one of the two (stable) roots of f: $u^{(0)} = u^{(0)\pm}$, where for Eq. (2a), $u^{(0)+} = 1$ and $u^{(0)-} = 0$. The field $v^{(0)}$ is time independent and is found by matching to the interface.

At lowest order (order ε^0 and order ε^{-1}), Eqs. (4) in the interface region give

$$0 = \frac{\partial^2 u^{i(0)\pm}}{\partial \bar{\xi}^2} + f(u^{i(0)\pm}, v^{i(0)\pm}), \tag{16}$$

$$0 = \partial v^{i(0)\pm} / \partial \bar{\xi}. \tag{17}$$

Here, the superscripts $\pm$ stand for interfaces $\Phi^\pm$. Matching $u^{i(0)\pm}$ to the solution in the outer region gives the boundary conditions on Eq. (16), $u^{i(0)\pm}(\bar{\xi} \to \pm\infty) = u^{\pm(0)}(\xi \to 0^\pm)$.

Equation (17) requires that $v^{i(0)\pm}$ not vary across the interface. Thus $v^{i(0)\pm}$ appearing in Eq. (16) is a constant. However, Eq. (16) will have a solution with the required boundary conditions only for one unique value of this constant. This value is known as the stall concentration, $v^{i(0)\pm} = v^s$. For Eqs. (2), $v^s = -b + a/2$. We assume that this constant is not of the order ε. Then the solution to Eq. (16) is $u^{i(0)\pm} = [1 \pm \tanh \bar{\xi}/(2\sqrt{2})]/2$, when the scroll interface is the surface $u = 1/2$ and the sense of $\bar{\xi}$ is given by the interface normals $\mathbf{N}^\pm$ as in Figs. 1 and 2.

Finally, the outer $v^{(0)}$ solution is obtained from matching to the interface solution $v^{i(0)\pm} = v^s$, $v^{(0)}(\xi \to 0^\pm) = v^{i(0)\pm}(\bar{\xi} \to \pm\infty)$. Since the interface passes through all points in the outer region at some time and since $v^{(0)}$ is independent of time [Eq. (15)], necessarily $v^{(0)}(r, \varphi, s) = v^s$. This completes the specification of the leading-order fields u and v everywhere outside the core.

C. First-order outer and interface regions

At ε^1 order, Eqs. (3) in the outer region give

$$0 = u^{(1)} f_u(u^{(0)\pm}, v^s) + v^{(1)} f_v(u^{(0)\pm}, v^s), \tag{18}$$

$$\partial v^{(1)} / \partial t = g^\pm(v^s), \tag{19}$$

where $g^\pm(v^s) \equiv g(u^{(0)\pm}, v^s)$ and subscripts denote derivatives. For the kinetics in Eqs. (2), $f_v(u^{(0)\pm}, v^s) = 0$, and hence Eq. (18) gives $u^{(1)} = 0$. [For kinetics (2), in the outer region $u^{(k)} = 0$ for all $k > 0$.] For these kinetics $g^\pm(v^s) = u^{(0)\pm} - v^s$.

Equations (4) in the interface at next order (order ε^1 and order ε^0) give

$$0=\frac{\partial^2 u^{i(1)\pm}}{\partial\bar{\xi}^2}+u^{i(1)\pm}f_u(u^{i(0)\pm},v^s)+v^{i(1)\pm}f_v(u^{i(0)\pm},v^s)+c^{\pm}\frac{\partial u^{i(0)\pm}}{\partial\bar{\xi}}, \tag{20}$$

$$0=\partial v^{i(1)\pm}/\partial\bar{\xi}, \tag{21}$$

where

$$c^{\pm}\equiv\mathbf{v}^{(0)\pm}\cdot\mathbf{N}^{\pm}-2H^{\pm}, \tag{22}$$

where $\mathbf{N}^{\pm}$ is the normal to, and $H^{\pm}$ is the mean curvature of, the leading-order interfaces $\Phi^{(0)\pm}$. Here, $\mathbf{v}^{(0)\pm}$ is the velocity in Eq. (5) for interfaces at leading order (from Sec. III A, the leading-order filament motion is zero). At leading order in our coordinates $\mathbf{v}^{(0)\pm}=r\dot{\Phi}^{(0)\pm}\mathbf{e}_{\varphi}^{\mathbf{s}\pm}$, and using the expression of the surface normal from the Appendix,

$$c^{\pm}=-r\dot{\Phi}^{(0)\pm}h^{\pm}/\sqrt{m^{\pm}}-2H^{\pm}, \tag{23}$$

where $m^{\pm}$ is the determinant of the metric tensor, and $h^{\pm}$ is the value of h, evaluated at the interfaces $\Phi^{(0)\pm}$. Matching $v^{i(1)\pm}$ to the outer solution requires $v^{i(1)\pm}(\bar{\xi}\to\pm\infty)=v^{(1)}(\xi\to 0^{\pm})$. From Eq. (21) $v^{i(1)\pm}$ does not vary across the interface; $v^{i(1)\pm}(\hat{r},\hat{s},\bar{\xi},t)=v^{i(1)\pm}(\hat{r},\hat{s},t)$. Thus $v^{i(1)\pm}=v^{(1)\pm}$, where $v^{(1)\pm}$ is the outer concentration $v^{(1)}$ at the interfaces $\Phi^{(0)\pm}$.

The general solution of Eq. (20) is obtained by a double variation of constants. This solution diverges for $\bar{\xi}\to\pm\infty$, in general. On both interfaces $\Phi^{(0)\pm}$, the required matching to the finite outer solution $u^{i(1)\pm}(\bar{\xi}\to\pm\infty)=u^{(1)}(\xi\to 0^{\pm})$ dictates a specific value of $c^{\pm}$. For Eqs. (2), the solution is simply $u^{i(1)\pm}=0$ and the value of $c^{\pm}$ is

$$c^{\pm}=\pm\frac{\sqrt{2}}{a}v^{i(1)\pm}. \tag{24}$$

(The $\pm$ signs arise here because of the sense of the interface normals we have defined. see Fig. 1.)

This leaves Eq. (19) for $v^{(1)}$ in the outer region together with the required boundary condition from matching that $v^{(1)}=v^{i(1)\pm}$ at the (moving) interfaces. Thus Eq. (19) and Eq. (24), together with $c^{\pm}$ obtained from Eq. (22), give finally the free-boundary equations

$$\partial v^{(1)}/\partial t=u^{\pm}-v^s, \tag{25}$$

$$-\frac{r\dot{\Phi}^{(0)\pm}h^{\pm}}{\sqrt{m^{\pm}}}=2H^{\pm}\pm\frac{\sqrt{2}}{a}v^{(1)\pm}. \tag{26}$$

Noting that in our coordinates the interface normal velocity is

$$\mathbf{v}^{(0)\pm}\cdot\mathbf{N}^{\pm}=-\frac{r\dot{\Phi}^{(0)\pm}h^{\pm}}{\sqrt{m^{\pm}}},$$

Eq. (26) equates the normal velocity of the interface to twice the mean curvature H of the interface plus the speed of a plane interface. This result for leading-order interface motion is widely known, e.g. Refs. [23–28,33], although in the context of excitable media it has been considered mainly in two-space dimensions. What is important here is that we express the free-boundary equations in a form appropriate for scroll waves in three-dimensional media using a system of coordinates based on the scroll filament. Explicit expressions for h, m, and H in these coordinates are given in the following section.

IV. EXAMPLES

In this section, we will apply the leading-order free-boundary equations (25) and (26) to important specific cases for which the equations simplify. We shall restrict our attention to cases in which scroll solutions do not depend on the coordinate s parametrizing the filament. This class of solutions includes twisted scrolls with straight filaments, axisymmetric scroll rings, and certain helical scrolls.

Frequently in this section we shall drop the superscripts, it being understood that all relevant quantities are evaluated on the leading-order interfaces $\Phi^{(0)\pm}$. When necessary, we shall distinguish the front and back interfaces; leading order is assumed throughout.

The general expressions for h, m, and H, which appear in Eq. (26) are (see the Appendix)

$$h=\sigma(1-r\kappa\cos\Phi), \tag{27}$$

$$m=(1+\Psi^2)h^2+r^2\chi^2, \tag{28}$$

$$H=\frac{1}{2m^{3/2}}[E(1+\Psi^2)-2Fr\chi\Psi+G(r^2\chi^2+h^2)], \tag{29}$$

where

$$E\equiv r\chi^2[-h\Psi+r\sigma\kappa\sin\Phi]+h^2\sigma\kappa[\Psi\cos\Phi+\sin\Phi]+r\chi\frac{\partial h}{\partial s}-rh\frac{\partial\chi}{\partial s}, \tag{30a}$$

$$F\equiv-\chi[h\Psi^2+\sigma-r\sigma\kappa\Psi\sin\Phi]-h\frac{\partial\Psi}{\partial s}, \tag{30b}$$

$$G\equiv-h(\Psi^3+\Psi+r\Psi_r)/r. \tag{30c}$$

We have used the definitions

$$\Psi\equiv r\partial\Phi/\partial r, \tag{31}$$

$$\chi\equiv\sigma\tau+\partial\Phi/\partial s. \tag{32}$$

A. Filament geometry and scroll twist

The geometry of filaments and the twist of scroll waves about these filaments is discussed in detail in several publications, e.g., Refs. [15,47,17,48]. The *twist* τ_w of a scroll

filament is the rate of angular rotation of the interface about the filament per unit arclength along the filament [15,47]. More specifically it is given by the value of $(1/\sigma)\partial\mathbf{N}/\partial s\cdot(\mathbf{t}\times\mathbf{N})$ on the filament. In our coordinates

$$\tau_w=\tau+\frac{1}{\sigma}\frac{\partial\Phi}{\partial s}(r\to 0),$$

i.e., $\tau_w=\chi(r\to 0)/\sigma$.

The twist is composed of two components: one component arising from the torsion τ of the filament and the associated rotation of the Frenet frame with displacement along the filament; the other component arising from the arclength derivative of phase Φ along the filament. Recall that Φ is measured with respect to the Frenet frame. In general, the instantaneous twist associated with the two interfaces Φ^+ and Φ^- need not be the same, $\partial\Phi^+/\partial s\neq\partial\Phi^-/\partial s$, in general. This possibility does not appear in past treatments of twisted scroll waves.

We are principally interested in solutions that do not depend on the coordinate s. For these the curvature and torsion of the filament must be constant. If both are nonzero the filament is helical. For concreteness, consider the filament to be parametrized as

$$\mathbf{X}(s)=(R\cos s, R\sin s, \gamma s).$$

The curvature and torsion are

$$\kappa=\frac{R}{R^2+\gamma^2},\quad \tau=\frac{\gamma}{R^2+\gamma^2}. \tag{33}$$

If $\gamma\to 0$ with finite R, one obtains a planar ring. In the limit $R\to 0$ one obtains a straight filament with twist. While the Frenet coordinates are undefined for a straight filament, it is possible to define the coordinate frame at $R=0$ by continuity.

We shall focus on s-independent situations for which $\partial\Phi^\pm/\partial s=0$. For such scroll waves the interfaces $\Phi^\pm$ are functions of r and t only: $\Phi^\pm(r,t)$. In this case the twist is the torsion, which in turn is a constant, and the two interfaces necessarily have the same twist. Finally, for this class of solutions, the s derivatives, Eqs. (30a) and (30b), drop out.

B. Numerical solutions

For the s-independent case, we can write the free-boundary equations (25) and (26) in terms of one two-dimensional field $v(r,\varphi)$ and two one-dimensional curves $\Phi^\pm(r)$, each depending on time according to

$$\frac{\partial v}{\partial t}=u^\pm-v^s, \tag{34}$$

$$\dot\Phi^\pm=\mp\frac{\sqrt{2}}{a}\frac{\sqrt{m^\pm}}{rh^\pm}v^\pm-\frac{2\sqrt{m^\pm}}{rh^\pm}H^\pm, \tag{35}$$

where v represents the first-order slow field $v^{(1)}$ and $v^\pm=v[r,\varphi=\Phi^\pm(r)]$ is its value at the $\pm$ interface. The quantities h, m, and H are given by Eqs. (27)–(28).

Equations (34) and (35) are easily simulated numerically. The v field is discretized on a polar grid of radius R_s with $N_r\times N_\varphi$ grid points. The center point at $r=0$ is not included, so that the domain begins at the first radial grid point $\Delta r=R_s/N_r$ from the center. In our simulations, we typically we use $\Delta r=0.05$ and 128 points in the φ direction. The interfaces $\Phi^\pm$ are represented using the same N_r radial grid points. The r derivatives in the interface equation are computed by finite differences with one-sided formulas used at the innermost and outermost grid points. The values of $v^\pm$ are found by interpolation of the v field.

Starting from an initial v field and valid (nonintersecting) interface curves, Eqs. (34) and (35) are simulated using the Euler time stepping until an asymptotic state, steady or time periodic, is reached.

C. Straight filament with constant twist

Consider first the simple case of a straight yet possibly twisted scroll. This is obtained as the limit $R\to 0$ in Eqs. (33). With our assumption of s independence, the twist τ_w is equal to the limiting value of the torsion.

With $\kappa=0$ the quantities occurring in the free-boundary equations simplify significantly to

$$h=1, \tag{36}$$

$$m=q+\Psi^2, \tag{37}$$

$$H=-\frac{1}{2(q+\Psi^2)^{3/2}}\left[\frac{\Psi(1+\Psi^2)}{r}+q\Psi_r\right], \tag{38}$$

where $q=1+\tau_w^2r^2$. For zero twist, $q=1$ and the problem reduces to the case of 2D spiral waves.

Figure 3 shows solutions to the free-boundary equations (34) and (35) for two values of twist. The solutions shown have reached a state of steady rotation.

One can derive a single universal equation for the shape and frequency of the steady (rigidly rotating) twisted scroll in Fig. 3. This has been done by Bernoff [37] in the general case and by Karma [35] for the zero-twist (i.e., 2D) case. One seeks a steady solution with (leading-order) frequency $\omega=\dot\Phi$, for which the angle between the wave front Φ^+ and wave back Φ^- is independent of r. In this case $\Psi\equiv r d\Phi/dr$ is the same for both interfaces. The angular separation between the two interfaces is found by integrating Eq. (25) in the quiescent $(-)$ and excited $(+)$ regions to give the change in $v^{(1)}$ between the interfaces, $\Delta v^{(1)}=v^{(1)+}-v^{(1)-}$. This is independent of r. Matching the change over the quiescent and excited regions, one finds that the angular separation between the interfaces is

$$\Delta\Phi\equiv\Phi^+-\Phi^-=2\pi v^s. \tag{39}$$

The separation is independent of twist.

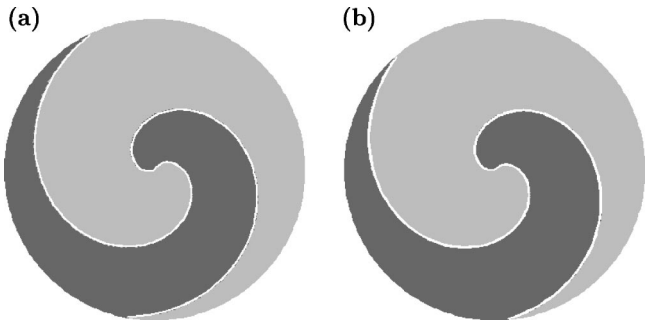

FIG. 3. Solutions of the free-boundary equations for a straight filament. (a) Untwisted scroll, i.e., a 2D spiral wave and (b) a twisted scroll with twist $\tau_w = 0.35$. Light (dark) gray areas denote the quiescent (excited) regions from the numerical solution of free-boundary equations (34) and (35). These time-asymptotic solutions rotate counterclockwise with constant frequency. The white curve is the interface obtained from universal equation (40). Parameters are $a = 1.0$, $b = 0.1$, and domain radius $R_s = 10$.

The values $v^{(1)\pm}$ can be eliminated from interface equation (26) to obtain a single universal equation describing the shape of the interface,

$$q\frac{d\Psi}{d\tilde{r}} + \frac{\Psi(1+\Psi^2)}{\tilde{r}} = \tilde{r}(q+\Psi^2) - B(q+\Psi^2)^{3/2}, \quad (40)$$

where lengths have been rescaled using the frequency $\tilde{r} \equiv \sqrt{\omega} r$, $\tilde{\tau}_w \equiv \tau_w/\sqrt{\omega}$. The value of q is unchanged, $q = 1 + \tau_w^2 r^2 = 1 + \tilde{\tau}_w^2 \tilde{r}^2$. The eigenvalue B is given by

$$B = (\mu/\omega)^{3/2}, \quad \mu^{3/2} = \sqrt{2}\,\pi v^s (1 - v^s)/a. \quad (41)$$

Equation (40) gives the leading-order shape Ψ and frequency, via B, of a twisted scroll wave with a straight filament. For zero twist ($q = 1$), the equation describes the leading-order shape of 2D spiral waves. Appropriate boundary conditions for solving Eq. (40) are obtained from the large-r asymptotics of the equation. Figure 3 shows a comparison of solutions to the universal equation and time-asymptotic solutions obtained by direct simulation of the free-boundary equations. Not surprisingly, the two solutions are indistinguishable. The rotation frequencies are also the same. Elsewhere [40,41], some solutions to Eq. (40) are compared with leading-order results obtained directly by solving Eqs. (1).

D. Axisymmetric scroll ring

The next important case is an axisymmetric scroll ring of radius R. This corresponds to $\gamma = 0$ in Eqs. (33). The torsion and twist are zero and $\kappa = 1/R$. We then obtain

$$h = 1 - r\kappa\cos\Phi, \quad (42)$$

$$m = (1+\Psi^2)h^2, \quad (43)$$

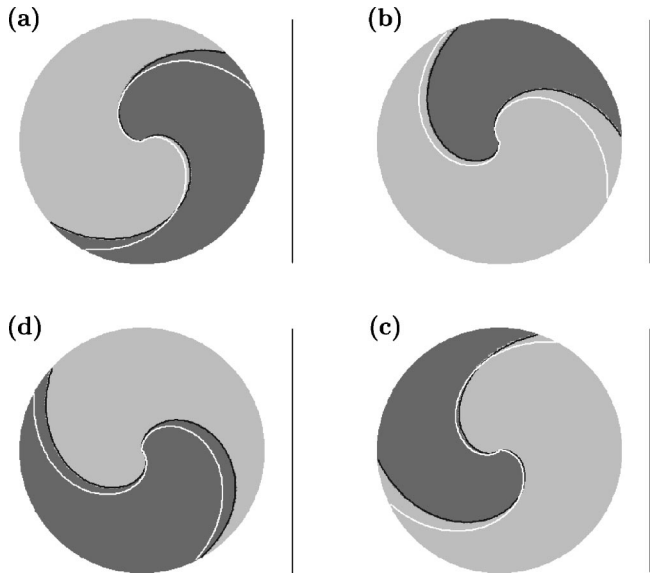

FIG. 4. Nonstationary rotation of an axisymmetric scroll ring from numerical solution of free-boundary equations (34) and (35). The plots show the solution at four equally spaced time intervals over the rotation period. The quiescent (light gray) and excited (dark gray) regions are separated by the numerically computed interfaces (thin black curves). The simulation domain of radius $R_s = 5$ is normal to the filament ring of radius $R = 6$. The symmetry axis of the scroll ring is to the right of the simulation domain as indicated. The white curve is the interface for a 2D spiral wave. Parameters are $a = 1.0$ and $b = 0.1$.

$$H = -\frac{1}{2(1+\Psi^2)^{3/2}}\left[\frac{\Psi(1+\Psi^2)}{r} + \Psi_r\right] + \frac{\kappa}{2\sqrt{1+\Psi^2}}\,\frac{\Psi\cos\Phi + \sin\Phi}{1 - r\kappa\cos\Phi}. \quad (44)$$

The polar coordinates in this description are only valid for $r\kappa = r/R < 1$. On substituting into the free-boundary equations, Eq. (35) for $\dot{\Phi}$ becomes

$$\dot{\Phi}^{\pm} = (2\text{D terms}) + \frac{\kappa}{r}\,\frac{\Psi^{\pm}\cos\Phi^{\pm} + \sin\Phi^{\pm}}{1 - r\kappa\cos\Phi^{\pm}}, \quad (45)$$

where the 2D terms are those which appear for spiral waves, or equivalently, a straight filament with zero twist.

Figure 4 shows the asymptotic, time-periodic evolution of an axisymmetric scroll ring obtained by numerically simulating free-boundary equations (34) and (35), starting from a 2D spiral-wave solution. The filament ring has radius $R = 6$ so that the curvature is $\kappa = 1/6$. The simulation domain of radius $R_s = 5$ is normal to the ring. The symmetry axis of the scroll ring is to the right of the simulation domain as indicated. Shown for comparison is the rigidly rotating 2D ($\kappa = 0$) solution to the free-boundary equations. It is also shown at four equally spaced time intervals over its rotation period. (The period of the $\kappa = 0$ is almost identical to the period of the scroll ring solution; see below.)

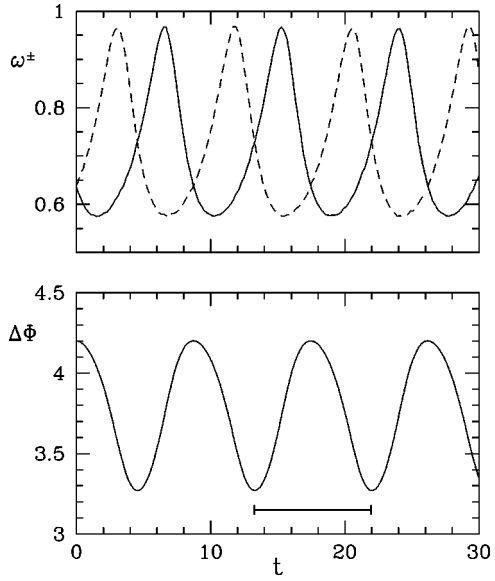

FIG. 5. Time series showing the instantaneous angular velocities of the interfaces, $\omega^{\pm}$ (top), and instantaneous separation of the interfaces, $\Delta\Phi$ (bottom), for the axisymmetric scroll solution shown in Fig. 4. The horizontal bar indicates one period of the $\kappa=0$ solution. Quantities are from the interfaces at half domain radius $r=R_s/2=2.5$.

With curvature, the interfaces do not have fixed shape. Instead, due to the explicit dependence of interface position Φ in the mean curvature, the interfaces move at speeds that depend on the position Φ about the curved filament. Hence the instantaneous angular velocities of the interfaces and their instantaneous angular separation vary periodically in time. We show this quantitatively in Fig. 5 by plotting these quantities extracted from the interfaces at half the domain radius, $R_s/2$. In this case it is not possible to reduce the free-boundary equations to a single time-independent universal equation, as has been done in the absence of curvature. Only for $\kappa=0$, the factors in $\cos\Phi$ and $\sin\Phi$ drop out of the free-boundary equations.

The filament of axisymmetric scroll solutions of the full reaction-diffusion equations (1) is known to be time dependent [10–12,9,15]. In general, the radius of axisymmetric scroll rings shrinks with time and the ring translates in a direction perpendicular to the plane of the ring. However, we stress that this motion is absent at leading order in ε (see Sec. III A). Hence the solutions in Fig. 4, in which there is no filament motion, are the correct dynamics of the reaction-diffusion equations at leading order in ε. The filament motion seen in laboratory and numerical experiments comes at higher order in ε.

The terms due to curvature in the free-boundary equations are of size $O(\kappa)$. Hence the fluctuations in the interface shape and instantaneous frequency seen in Figs. 4 and 5 are of this order. This is shown quantitatively in Figs. 5 and 6, where we show results from a simulation with $\kappa=1/6$ and $\kappa=1/12$. The magnitude of fluctuations for $\kappa=1/12$ is almost exactly half of that found for $\kappa=1/6$.

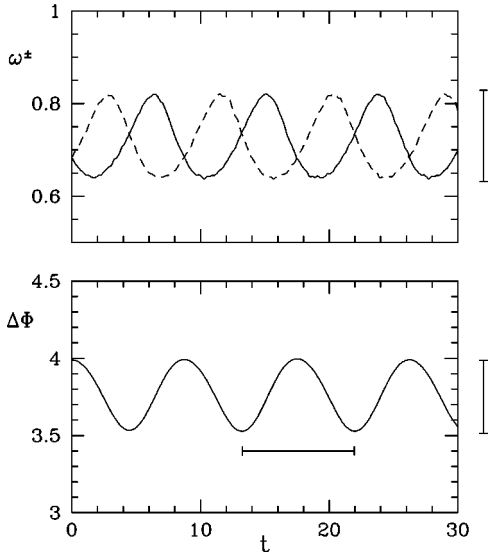

FIG. 6. Same as Fig. 5 except that the scroll ring has radius $R=12$, i.e., half the curvature. The vertical bars to the right show half the peak-to-peak variation of the $R=6$ case. The horizontal bar indicates one period of the $\kappa=0$ solution.

What is of particular interest is the effect of curvature on the (mean) frequency and on the average interface shape. For this we consider the limit of small curvature and average the free-boundary equations over one period of the zero-curvature solution. It is most convenient to work in the rotating reference frame for which the $\kappa=0$ solution is time independent:

$$\tilde{\varphi}=\varphi-\omega t,$$

$$\tilde{v}(r,\tilde{\varphi})=v(r,\varphi-\omega t),$$

$$\tilde{\Phi}^{\pm}(r)=\Phi^{\pm}(r,t)-\omega t.$$

In the rotating coordinates, the curvature term in Eq. (45) is, at lowest order in κ,

$$\frac{\kappa}{r}\{\Psi^{\pm}(r)\cos[\tilde{\Phi}^{\pm}(r)+\omega t]+\sin[\tilde{\Phi}^{\pm}(r)+\omega t]\}.$$

The average of this term over one period of the unperturbed problem is zero, i.e., there are no resonant terms at the leading order. Curvature does not explicitly enter the equation for the slow field. Thus, to $O(\kappa)$, the average equations for the axisymmetric scroll ring are the same as the equations for a 2D spiral wave. As a result, the rotation period of an an axisymmetric scroll ring can be expected to be quite close to that of the 2D spiral wave with the same kinetics parameters. This can be seen in Figs. 5 and 6 where the mean rotation period in both cases is very close to the period of the 2D spiral wave for the same conditions. Verification of the $O(\kappa^2)$ scaling is beyond the precision of the numerical scheme we have used. The mean interface separation is almost exactly that for a 2D spiral wave.

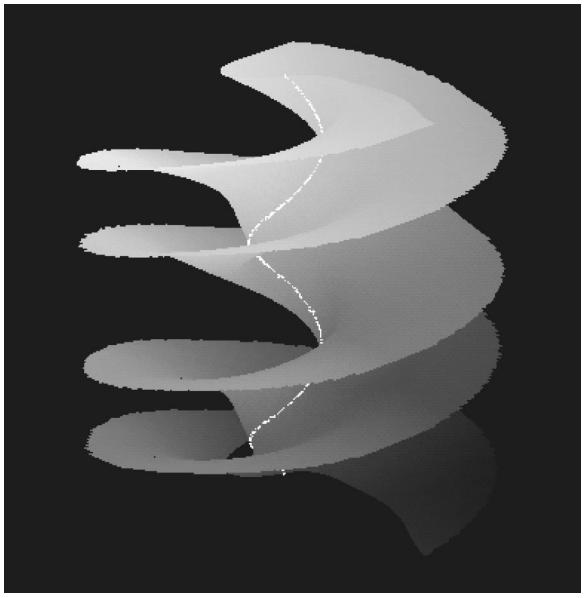

FIG. 7. Symmetric helix from numerical solution of Eqs. (1) and (2). The isosurfaces of the u field are shown corresponding to the interfaces Φ^+ and Φ^-. The helical filament is shown in white. The parameters are $a=1.0$, $b=0.1$, and $\varepsilon=0.2$

E. Symmetric helix

Our final example is a scroll with a helical filament. We shall call an s-independent scroll wave with a helical filament a symmetric helix, in analogy with the axisymmetric scroll ring. Figure 7 shows such a state obtained from solution of the full reaction-diffusion equations (1) and (2). The twist of the scroll is equal to the torsion and so the scroll phase rotates exactly as does the Frenet coordinate frame. This helix arises from an instability of a straight, twisted filament (so-called sproing instability). Such helices have been studied numerically and analytically in the framework of filament dynamics [49,17,48].

Figure 8 shows results from simulations of the free-boundary equations (34) and (35) for such a helix. The twist is $\tau_w=0.35$, the same value is shown for the twisted straight filament in Fig. 3; the curvature is $\kappa=1/6$. The normal and binormal directions are horizontal and vertical, respectively. Simulations are started from a solution for a straight, twisted scroll and evolved until an asymptotic periodic solution is reached. As for the scroll ring, the interfaces are not of fixed shape during rotation.

For the helix, the expressions for h, m, and H appear in the interface equation (35) and do not simplify significantly from the general expressions (27) and (28), so we do not give them here. However, for small curvature, the interface equation is of the form

$$\dot{\Phi}^{\pm}=(\text{Straight terms})+\kappa[A_1(\Psi^{\pm},\Psi_r^{\pm},r,\tau_w,v^{\pm})\cos\Phi^{\pm} + A_2(\Psi^{\pm},r,\tau_w)\sin\Phi^{\pm}]+O(\kappa^2),$$

where the straight terms are those appearing in the equation for the straight filament with twist τ_w, and A_1 and A_2 are functions of the arguments shown.

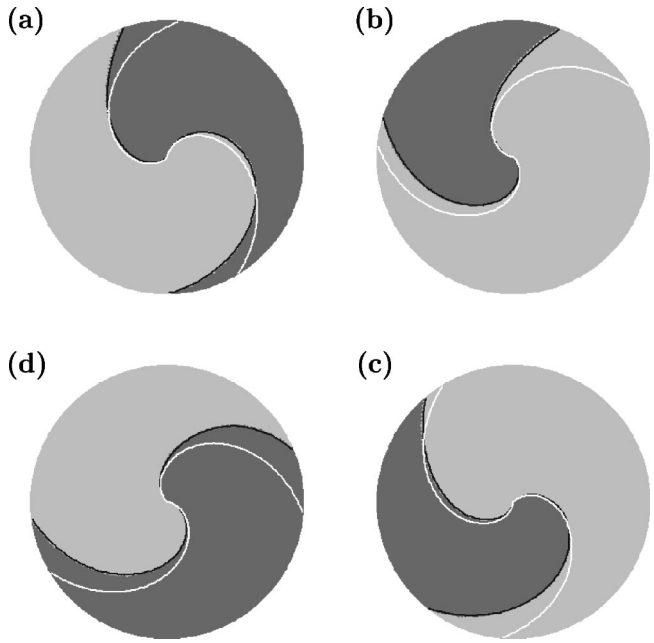

FIG. 8. Nonstationary rotation of a helical scroll wave from numerical solution of free-boundary equations (34) and (35). The plots show the solution at four equally spaced time intervals over the rotation period. The quiescent (light gray) and excited (dark gray) regions are separated by the numerically computed interface (thin black curve). The simulation domain of radius $R_s=5$ is normal to the filament for which $\kappa=1/6$ and $\tau_w=0.35$. The white curve is the interface for a straight scroll with $\tau_w=0.35$. Parameters are $a=1.0$ and $b=0.1$.

The interface equation contains $O(\kappa)$ terms and so the periodic variation in the interface speed and shape seen in Fig. 8 are of $O(\kappa)$, just as for the scroll ring previously shown. The $O(\kappa)$ terms have zero mean and so the average of the $\dot{\Phi}$ equation is the same as the equation for a straight filament with twist up to $O(\kappa^2)$ terms. Thus the mean interface shape and frequency can be predicted from the solution of universal equation (40) up to $O(\kappa^2)$. We find that the numerically computed rotation period of the free-boundary solution shown in Fig. 8 is almost identical to the period of the straight twisted scroll shown in Fig. 3(b).

V. CORE EQUATIONS

We return now to the equations in the core region. Solutions in this region are necessary to provide a complete asymptotic solution to the reaction-diffusion equations everywhere in space. In particular, the solution in the core region is necessary to regularize the cusp that would otherwise exist in most cases as the wave front Φ^+ and wave back Φ^- come together in the vicinity of the filament. Unfortunately, the core equations cannot be reduced to one dimension and hence must be solved numerically with boundary conditions determined from the outer solutions. Kessler *et al.* [36,39] have done this in the 2D steady case. Fortunately, for steady spiral waves in 2D and for the examples in the preceding section, core solutions do not dictate the leading-order frequency or interface shape. Hence, with regard to the impor-

tant issues of selection of rotation frequency and scroll shape, explicit core solutions are not required. For completeness we shall give the core equations at leading and first order (the lowest order for which filament curvature enters the core equations), but we shall not give solutions to these equations.

At order ε^0, Eqs. (11) for the fields in the core region are

$$0=\overline{\nabla}^{2c(0)}u^{c(0)}+f(u^{c(0)},v^{c(0)}), \tag{46}$$

$$\partial v^{c(0)}/\partial t=\mathcal{N}^{(0)}\equiv\dot{\mathbf{X}}^{(1)}\cdot\overline{\boldsymbol{\nabla}}^{c(0)}v^{c(0)}, \tag{47}$$

where $\overline{\boldsymbol{\nabla}}^{c(0)}$ is defined in Eq. (13), and

$$\overline{\nabla}^{2c(0)}\equiv\frac{\partial^2}{\partial\overline{r}^2}+\frac{1}{\overline{r}}\frac{\partial}{\partial\overline{r}}+\frac{1}{\overline{r}^2}\frac{\partial^2}{\partial\varphi^2}.$$

Asymptotic matching to the outer region gives the boundary conditions $v^{c(0)}(\overline{r}\to\infty)=v^{(0)}(r\to 0)=v^s$ and $u^{c(0)}(\overline{r}\to\infty)=u^{\pm(0)}(r\to 0)$.

At order ε^1, Eqs. (11) give

$$\overline{\nabla}^{2c(0)}u^{c(1)}+u^{c(1)}f_u(u^{c(0)},v^{c(0)})=\mathcal{M}^{(1)}, \tag{48}$$

$$\partial v^{c(1)}/\partial t=g(u^{c(0)},v^{c(0)})+\mathcal{N}^{(1)}, \tag{49}$$

where

$$\mathcal{M}^{(1)}=-v^{c(1)}f_v(u^{c(0)},v^{c(0)})+\kappa\overline{\nabla}^{c(0)}u^{c(0)}\cdot\mathbf{n},$$

$$\mathcal{N}^{(1)}=(\dot{\mathbf{X}}^{(2)}+\overline{r}\dot{\mathbf{e}}_r^{(1)})\cdot\overline{\nabla}^{c(0)}v^{c(0)}+\dot{\mathbf{X}}^{(1)}\cdot\overline{\nabla}^{c(0)}v^{c(1)}+\mathbf{t}\cdot\dot{\mathbf{X}}^{(1)}\mathcal{H}^{(0)}v^{c(0)},$$

where

$$\mathcal{H}^{(0)}\equiv\frac{1}{\sigma}\left(\frac{\partial}{\partial s}-\sigma\tau\frac{\partial}{\partial\varphi}\right).$$

In order to close the steady version of Eqs. (46) and (47) for the steady spiral in 2D, Kessler *et al.* [36,39] have extracted a compatibility condition from the steady version of Eq. (49).

In the same way, in order to close the steady version of Eqs. (48) and (49) for the steady spiral in 2D, one needs to extract a compatibility condition from the equation for the v field at next order. This next order equation is

$$\partial v^{c(2)}/\partial t=u^{c(1)}-v^{c(1)}+\mathcal{N}^{(2)}, \tag{50}$$

where

$$\mathcal{N}^{(2)}=(\dot{\mathbf{X}}^{(3)}+\overline{r}\dot{\mathbf{e}}_r^{(2)})\cdot\overline{\nabla}^{c(0)}v^{c(0)}+(\dot{\mathbf{X}}^{(2)}+\overline{r}\dot{\mathbf{e}}_r^{(1)})\cdot\overline{\nabla}^{c(0)}v^{c(1)}+\dot{\mathbf{X}}^{(1)}\cdot\overline{\nabla}^{c(0)}v^{c(2)}+\mathbf{t}\cdot(\dot{\mathbf{X}}^{(2)}+\overline{r}\dot{\mathbf{e}}_r^{(1)})\mathcal{H}^{(0)}v^{c(0)}+\mathbf{t}\cdot\dot{\mathbf{X}}^{(1)}(\mathcal{H}^{(0)}v^{c(1)}+\overline{r}\kappa\cos\varphi\mathcal{H}^{(0)}v^{c(0)}).$$

These expressions show explicitly how the curvature and filament motion enter the equations for the core region. The differences between these equations, for a moving curved scroll filament, and the core equations for a stationary 2D spiral (straight motionless filament) are the curvature term $\kappa\overline{\nabla}^{c(0)}u^{c(0)}\cdot\mathbf{n}$ in the expression of $\mathcal{M}^{(1)}$ and the terms containing the time derivatives of the filament position at first and second order, $\dot{\mathbf{X}}^{(1)}$ and $\dot{\mathbf{X}}^{(2)}$. In addition, because curvature dictates a nonstationary outer solution, curvature affects core solutions in a nontrivial way via the boundary conditions on the core obtained by matching to the outer solution.

VI. CONCLUSIONS

We have presented a systematic, order-by-order approach to a full matched asymptotic description of scroll waves in excitable media in the large-excitability (small-ε) limit. A large part of our purpose has been to specify a useful system of coordinates for the free-boundary equations in three dimensions. These coordinates are a natural extension of coordinates used to study spirals in two dimensions and they provide nice coordinates for numerical simulations. We have considered some specific examples in which the free-boundary equations simplify and we have shown numerical solutions to these equations. While we have focused on a particular model, our approach can be readily applied to all similar models of excitable media as in Refs. [35,37]. Comparisons with full solutions to the reaction-diffusion equations are presented elsewhere [40,41].

The derivation of the free-boundary equations does not require the assumption that filament curvature and twist are small. The operators appearing in our equations are, in fact, simpler than those in the singular-perturbation approach pioneered by Keener *et al.* [14,16,18]. By considering the small-ε limit first, we thus are able to treat scroll waves whose filaments have large (order-one) curvature, and moreover, we are able to capture the $O(\kappa)$ variations in interface motion arising because of curvature.

The way in which the difficulty of curvature enters our approach is that curvature eliminates the possibility of exactly stationary (rigidly rotating) solutions of the free-boundary equations. Thus exact order-by-order solutions are not stationary even in the small-ε limit and this presents very difficult challenges for obtaining solutions to the asymptotic equations. Nevertheless, it would be of interest to consider formally the small-curvature limit of the equations we have obtained. Because the large-excitability limit results in considerable simplifications, we may hope that in these two limits it will be possible to make progress on the problem of filament motion. In particular, there is hope that equations of slow filament motion may be obtained in which coefficients are directly related to parameters of the original reaction-diffusion equations.

APPENDIX: COORDINATE SYSTEMS

In this appendix we give some useful properties of the coordinate systems used. We base our derivation on the Frenet equations

$$\frac{\partial \mathbf{X}}{\partial s}=\sigma\mathbf{t}, \quad \frac{\partial \mathbf{t}}{\partial s}=\sigma\kappa\mathbf{n},$$

$$\frac{\partial \mathbf{n}}{\partial s}=\sigma(\tau\mathbf{b}-\kappa\mathbf{t}), \quad \frac{\partial \mathbf{b}}{\partial s}=-\sigma\tau\mathbf{n},$$

where τ is the torsion and κ the curvature of the curve (filament) given parametrically by $\mathbf{X}(s)$, and $\sigma\equiv|\partial\mathbf{X}/\partial s|$.

1. Outer coordinates

A point $\mathbf{x}$ in coordinates (r,φ,s) is given by $\mathbf{x}=\mathbf{X}(s)+r\mathbf{e}_r(\varphi,s)$, where $\mathbf{e}_r=\cos\varphi\mathbf{n}+\sin\varphi\mathbf{b}$. The coordinate frame $(\mathbf{E}_1,\mathbf{E}_2,\mathbf{E}_3)$ for (r,φ,s) is

$$\mathbf{E}_1=\mathbf{e}_r,$$

$$\mathbf{E}_2=r\partial\mathbf{e}_r/\partial\varphi=r\mathbf{e}_\varphi,$$

$$\mathbf{E}_3=\frac{\partial\mathbf{X}}{\partial s}+r\frac{\partial\mathbf{e}_r}{\partial s}=h\mathbf{t}+r\sigma\tau\mathbf{e}_\varphi,$$

where $h\equiv\sigma(1-r\kappa\cos\varphi)$. Hence the (r,φ,s) coordinates are not an orthogonal system.

The expressions for the gradient and Laplacian operators in (r,φ,s) coordinates can, however, be easily deduced by using the orthogonal coordinates $(r,\theta=\varphi+\int_0^s\sigma\tau ds',s)$ and the associated change of variables,

$$\frac{\partial}{\partial\theta}=\frac{\partial}{\partial\varphi}, \quad \left.\frac{\partial}{\partial s}\right|_\theta=\left.\frac{\partial}{\partial s}\right|_\varphi-\sigma\tau\frac{\partial}{\partial\varphi}. \tag{A1}$$

The coordinate frame for (r,θ,s) is

$$\mathbf{E}_1=\mathbf{e}_r,$$

$$\mathbf{E}_2=r\partial\mathbf{e}_r/\partial\theta=r\partial\mathbf{e}_r/\partial\varphi=r\mathbf{e}_\varphi,$$

$$\mathbf{E}_3=\frac{\partial\mathbf{X}}{\partial s}+r\left.\frac{\partial\mathbf{e}_r}{\partial s}\right|_\theta=\sigma\mathbf{t}+r\left.\frac{\partial\mathbf{e}_r}{\partial s}\right|_\varphi-r\sigma\tau\frac{\partial\mathbf{e}_r}{\partial\varphi}=h\mathbf{t}.$$

The components m_{ij} of the metric tensor for these orthogonal coordinates are thus $m_{11}=1$, $m_{22}=r^2$, and $m_{33}=h^2$.

The representation for the gradient and Laplacian operators in orthogonal coordinates are standard. From their representation in (r,θ,s) coordinates, one can use Eq. (A1) to obtain their representation in the nonorthogonal (r,φ,s) coordinates.

2. Interface coordinates

We consider properties of the local interface coordinates $(\hat r,\hat s,\xi)$ and, in particular, give properties of the coordinates at the surface (interface) $\xi=0$. Where necessary we shall distinguish intrinsic surface quantities from similar volume quantities by the superscript **s**. We also use superscript **s** to indicate volume quantities evaluated at the surface. In the main part of the paper this superscript is rarely used; surface quantities are clear either from accompanying text or the use of the superscript $\pm$ denoting wave front/back.

In general, for a surface given parametrically as $\mathbf{x}^{\mathbf{s}}(x_1,x_2)$, the surface tangent vectors $\mathbf{E}_i^{\mathbf{s}}=\partial\mathbf{x}/\partial x_i$ define the surface coordinate bases with corresponding metric tensor $m_{ij}^{\mathbf{s}}=\mathbf{E}_i^{\mathbf{s}}\cdot\mathbf{E}_j^{\mathbf{s}}$. If the interface is described by the two parameters $(x_1,x_2)=(\hat r,\hat s)$, as $\mathbf{x}^{\mathbf{s}}=\mathbf{X}(\hat s)+\hat r\mathbf{e}_r[\Phi(\hat r,\hat s),\hat s]$, then

$$\mathbf{E}_1^{\mathbf{s}}=\mathbf{e}_r^{\mathbf{s}}+\Psi\mathbf{e}_\varphi^{\mathbf{s}},$$

$$\mathbf{E}_2^{\mathbf{s}}=\hat r\chi\mathbf{e}_\varphi^{\mathbf{s}}+h^{\mathbf{s}}\mathbf{t},$$

$$m_{11}^{\mathbf{s}}=1+\Psi^2,$$

$$m_{22}^{\mathbf{s}}=\hat r^2\chi^2+(h^{\mathbf{s}})^2,$$

$$m_{12}^{\mathbf{s}}=m_{21}^{\mathbf{s}}=\hat r\Psi\chi,$$

$$m^{\mathbf{s}}=m_{11}^{\mathbf{s}}m_{22}^{\mathbf{s}}-(m_{12}^{\mathbf{s}})^2=(1+\Psi^2)(h^{\mathbf{s}})^2+\hat r^2\chi,$$

where $h^{\mathbf{s}}=\sigma(1-\hat r\kappa\cos\Phi)$, $\Psi=\hat r\Phi_{\hat r}$, $\chi=\sigma\tau+\Phi_{\hat s}$, $\mathbf{e}_r^{\mathbf{s}}=\mathbf{e}_r[\Phi(\hat r,\hat s),\hat s]$, $\mathbf{e}_\varphi^{\mathbf{s}}=\mathbf{e}_\varphi[\Phi(\hat r,\hat s),\hat s]$, and $m^{\mathbf{s}}$ is the determinant of the metric tensor.

The 3D local coordinates $(\hat r,\hat s,\xi)$ are such that points $\mathbf{x}$ near the surface $(\hat r,\hat s,\xi)$ are given by $\mathbf{x}=\mathbf{x}^{\mathbf{s}}+\xi\mathbf{N}$, where $\mathbf{N}$ is the unit normal to the surface. The coordinate frame $(\mathbf{E}_1,\mathbf{E}_2,\mathbf{E}_3)$ associated to $(\hat r,\hat s,\xi)$ can be expressed in terms of the interface coordinate frame $(\mathbf{E}_1^{\mathbf{s}},\mathbf{E}_2^{\mathbf{s}})$ via

$$\mathbf{E}_1=(1-\xi L_1^1)\mathbf{E}_1^{\mathbf{s}}-\xi L_1^2\mathbf{E}_2^{\mathbf{s}}\equiv h_{11}\mathbf{E}_1^{\mathbf{s}}+h_{12}\mathbf{E}_2^{\mathbf{s}},$$

$$\mathbf{E}_2=-\xi L_2^1\mathbf{E}_1^{\mathbf{s}}+(1-\xi L_2^2)\mathbf{E}_2^{\mathbf{s}}\equiv h_{21}\mathbf{E}_1^{\mathbf{s}}+h_{22}\mathbf{E}_2^{\mathbf{s}},$$

$$\mathbf{E}_3=\mathbf{N}=\mathbf{E}_1^{\mathbf{s}}\times\mathbf{E}_2^{\mathbf{s}}/|\mathbf{E}_1^{\mathbf{s}}\times\mathbf{E}_2^{\mathbf{s}}|,$$

with $L_i^k=\Sigma_j L_{ij}m^{\mathbf{s}kj}$, for $i,j,k=1,2$, where $L_{ij}=\partial\mathbf{E}_i^{\mathbf{s}}/\partial x_j\cdot\mathbf{N}$ are the fundamental forms and $m^{\mathbf{s}ij}$ are the components of the inverse of the surface metric tensor. We have used the Weingarten theorem [50]:

$$\frac{\partial\mathbf{N}}{\partial x_i}=-\sum_k L_i^k\mathbf{E}_k^{\mathbf{s}}.$$

The unit normal is

$$\mathbf{N}=(h^{\mathbf{s}}\Psi\mathbf{e}_r^{\mathbf{s}}-h^{\mathbf{s}}\mathbf{e}_\varphi^{\mathbf{s}}+\hat r\chi\mathbf{t})/m^{\mathbf{s}1/2}.$$

The components of the metric tensor associated to the coordinates $(\hat r,\hat s,\xi)$ are

$$m_{11}=m_{11}^{\mathbf{s}}h_{11}^2+2m_{12}^{\mathbf{s}}h_{12}h_{11}+m_{22}^{\mathbf{s}}h_{12}^2,$$

$$m_{22}=m_{11}^{\mathbf{s}}h_{21}^2+2m_{12}^{\mathbf{s}}h_{21}h_{22}+m_{22}^{\mathbf{s}}h_{22}^2,$$

$$m_{33}=1,$$

$$m_{12}=m_{21}=m^{\mathbf{s}}_{11}h_{11}h_{21}+m^{\mathbf{s}}_{12}(h_{11}h_{22}+h^2_{12})+m^{\mathbf{s}}_{22}h_{12}h_{22},$$

$$m_{13}=m_{31}=m_{23}=m_{32}=0,$$

and the determinant is $m=m_{11}m_{22}-m^2_{12}$.

The gradient operator is

$$\boldsymbol{\nabla} u=\sum_{i,j=1}^{2} m^{ij}\frac{\partial u}{\partial x_j}\mathbf{E}_i+\frac{\partial u}{\partial \xi}\mathbf{N}\equiv\boldsymbol{\nabla}_{\pi}u+\frac{\partial u}{\partial \xi}\mathbf{N},$$

and the Laplacian is

$$\nabla^2 u=\frac{1}{m^{1/2}}\sum_{i,j=1}^{2}\frac{\partial}{\partial x_j}\left(m^{1/2}m^{ij}\frac{\partial u}{\partial x_i}\right)+\frac{1}{m^{1/2}}\frac{\partial}{\partial \xi}\left(m^{1/2}\frac{\partial u}{\partial \xi}\right)$$

$$\equiv\nabla^2_{\pi}u+\frac{\partial^2 u}{\partial \xi^2}+\frac{1}{2m}\frac{\partial m}{\partial \xi}\frac{\partial u}{\partial \xi},\qquad\text{(A2)}$$

where m^{ij} are the components of the inverse metric tensor.

We need the last term in Eq. (A2) at leading order in ξ, which will be leading order in ε when using the stretched coordinate $\bar{\xi}=\xi/\varepsilon$. Expanding the m_{ij} using the definitions of h_{ij} gives

$$m_{11}=m^{\mathbf{s}}_{11}-2\xi L_{11}+O(\xi^2),$$

$$m_{22}=m^{\mathbf{s}}_{22}-2\xi L_{22}+O(\xi^2),$$

$$m_{12}=m^{\mathbf{s}}_{12}-2\xi L_{12}+O(\xi^2).$$

Thus

$$m=m_{11}m_{22}-m^2_{12}=m^{\mathbf{s}}+\xi m_1+O(\xi^2),$$

where

$$m_1=-2(m^{\mathbf{s}}_{11}L_{22}-2m^{\mathbf{s}}_{12}L_{12}+m^{\mathbf{s}}_{22}L_{11}).$$

Therefore

$$\frac{1}{2m}\frac{\partial m}{\partial \xi}=\frac{m_1}{2m^{\mathbf{s}}}+O(\xi)=-2H+O(\xi),$$

where H is the mean curvature of the interface and is given by [50]

$$H=\frac{m^{\mathbf{s}}_{11}L_{22}-2m^{\mathbf{s}}_{12}L_{12}+m^{\mathbf{s}}_{22}L_{11}}{2m^{\mathbf{s}}}.$$

[1] A.N. Zaikin and A.M. Zhabotinsky, Nature (London) **225**, 535 (1970).
[2] A.T. Winfree, Science **175**, 634 (1972).
[3] J. Lechleiter, S. Girard, E. Peralta, and D. Clapham, Science **252**, 123 (1991).
[4] S. Nettesheim *et al.*, J. Chem. Phys. **98**, 9977 (1993).
[5] A. T. Winfree, *When Time Breaks Down* (Princeton University Press, Princeton, 1987).
[6] J.M. Davidenko *et al.*, Nature (London) **355**, 349 (1992).
[7] F.X. Witkowski *et al.*, Nature (London) **392**, 78 (1998).
[8] A.T. Winfree, Chaos **8**, 1 (1998).
[9] A.V. Panfilov, A.N. Rudenko, and V.I. Krinskii, Biofizika **31**, 850 (1986).
[10] A.V. Panfilov and A.N. Rudenko, Physica D **28**, 215 (1987).
[11] W. Jahnke, C. Henze, and A.T. Winfree, Nature (London) **336**, 662 (1988).
[12] A.T. Winfree and W. Jahnke, J. Phys. Chem. **93**, 2823 (1989).
[13] A.T. Winfree, Physica D **84**, 126 (1995).
[14] J.P. Keener, Physica D **31**, 269 (1988).
[15] A.T. Winfree, SIAM Rev. **32**, 1 (1990).
[16] J.P. Keener and J.J. Tyson, SIAM Rev. **34**, 1 (1992).
[17] A. T. Winfree, in *Chemical Waves and Patterns*, edited by R. Kapral and K. Showalter (Kluwer, London, 1995), pp. 3–5.
[18] V.N. Biktashev, A.V. Holden, and H. Zhang, Philos. Trans. R. Soc. London, Ser. A **347**, 611 (1994).
[19] P. C. Fife, in *Non-Equilibrium Dynamics in Chemical Systems*, edited by C. Vidal and A. Pacault (Springer-Verlag, Berlin, 1984), pp. 76–88.
[20] D. Barkley, M. Kness, and L.S. Tuckerman, Phys. Rev. A **42**, 2489 (1990).
[21] D. Barkley, Physica D **49**, 61 (1991).
[22] M. Dowle, R.M. Mantel, and D. Barkley, Int. J. Bifurcation Chaos Appl. Sci. Eng. **7**, 2529 (1997).
[23] H. Yamada and K. Nozaki, Physica D **64**, 153 (1993).
[24] H. Yamada and K. Nozaki, J. Phys. Soc. Jpn. **63**, 379 (1994).
[25] R.C. Brower, D.A. Kessler, J. Koplik, and H. Levine, Phys. Rev. A **29**, 1335 (1984).
[26] P.K. Brazhnik, V.A. Davydov, V.S. Zykov, and A.S. Mikhailov, Zh. Eksp. Teor. Fiz. **93**, 1725 (1987) [Sov. Phys. JETP **66**, 984 (1987)].
[27] A.S. Mikhailov and V.S. Zykov, Physica D **52**, 379 (1991).
[28] D. Ding, Physica D **32**, 471 (1988).
[29] V.N. Biktashev, Physica D **36**, 167 (1989).
[30] P.C. Fife, J. Stat. Phys. **39**, 687 (1985).
[31] J.P. Keener, SIAM (Soc. Ind. Appl. Math.) J. Appl. Math. **46**, 1039 (1986).
[32] J.P. Keener and J.J. Tyson, Physica D **21**, 307 (1986).
[33] J.J. Tyson and J.P. Keener, Physica D **32**, 327 (1988).
[34] J.P. Keener, SIAM (Soc. Ind. Appl. Math.) J. Appl. Math. **52**, 1370 (1992).
[35] A. Karma, Phys. Rev. Lett. **68**, 397 (1992).
[36] D.A. Kessler, H. Levine, and W.N. Reynolds, Phys. Rev. Lett. **68**, 401 (1992).
[37] A. Bernoff, Physica D **53**, 125 (1991).
[38] D.A. Kessler, H. Levine, and W. Reynolds, Phys. Rev. A **46**, 5264 (1992).
[39] D.A. Kessler, H. Levine, and W. Reynolds, Physica D **70**, 115 (1994).
[40] D. Margerit and D. Barkley, Phys. Rev. Lett. **86**, 175 (2001).
[41] D. Margerit and D. Barkley, Chaos **12**, 636 (2002).
[42] I. Aranson, D.A. Kessler, and I. Mitkov, Physica D **85**, 142 (1995).
[43] I. Mitkov, I. Aranson, and D.A. Kessler, Phys. Rev. E **52**, 5974 (1995).

[44] V. Hakim and A. Karma, Phys. Rev. Lett. **79**, 665 (1997).
[45] V. Hakim and A. Karma, Phys. Rev. E **60**, 5073 (1999).
[46] A. Karma, Phys. Rev. Lett. **66**, 2274 (1991).
[47] J.J. Tyson and S.H. Strogatz, Int. J. Bifurcation Chaos Appl. Sci. Eng. **1**, 723 (1991).
[48] J. J. Tyson and J. P. Keener, in *Chemical Waves and Patterns*, edited by R. Kapral and K. Showalter (Kluwer, Dordrecht, 1995), pp. 93–118.
[49] C. Henze, E. Lugosi, and A. Winfree, Can. J. Phys. **68**, 683 (1990).
[50] J. J. Stoker, *Differential Geometry*, Pure and Applied Mathematics Vol. 20 (Wiley, New York, 1989).